

Dynamical Axions in $U(1)$ Quantum Spin Liquids

Salvatore D. Pace,^{1,2} Claudio Castelnovo,² and Chris R. Laumann³

¹*Department of Physics, Massachusetts Institute of Technology, Cambridge, Massachusetts 02139, USA*

²*TCM Group, Cavendish Laboratory, University of Cambridge, Cambridge CB3 0HE, United Kingdom*

³*Department of Physics, Boston University, Boston, Massachusetts 02215, USA*

(Dated: July 22, 2022)

Since their proposal nearly half a century ago, physicists have sought axions in both high energy and condensed matter settings. Despite intense and growing efforts, to date experimental success has been limited, with the most prominent results arising in the context of topological insulators. Here we propose a novel mechanism whereby axions can be realized in quantum spin liquids. We discuss the necessary symmetry requirements and identify possible experimental realizations in candidate pyrochlore materials, such as $\text{Ba}_3\text{Yb}_2\text{Zn}_5\text{O}_{11}$. In this context, the axions couple *both* to the external and to the emergent electromagnetic fields. We show that the interaction between the axion and the emergent photon leads to a characteristic dynamical response, which can be measured experimentally in inelastic neutron scattering. This work sets the stage for studying axion electrodynamics in the highly tunable setting of frustrated magnets.

Quantum spin liquids (QSL) are long-range entangled phases of matter where spins fractionalize and give rise to an emergent gauge structure [1–3]. One of the most fascinating examples is a $U(1)$ QSL, where the gauge structure is akin to quantum electrodynamics [4, 5]. Vastly different from our universe, this emergent quantum electrodynamics violates Lorentz symmetry, is strongly coupled, and contains magnetic monopoles. Such $U(1)$ QSLs have attracted substantial interest due to proposed experimental realizations [6–8] in a class of frustrated quantum rare-earth pyrochlore magnets known as quantum spin ice [9–15].

The long-wavelength effective description of a $U(1)$ QSL in 3+1D with only gapped matter is in terms of an emergent deconfined $U(1)$ vector gauge field whose quanta are gapless emergent photons, electric gauge charges that correspond to fractionalized excitations of the spins (spinons), and dual magnetic monopoles (visons) [16]. At energies lower than the matter gap, the universal properties of $U(1)$ QSL phases stem from their emergent photons governed by the Maxwell Lagrangian $\mathcal{L}_\gamma = (|\mathbf{e}|^2 - |\mathbf{b}|^2)/2$, where \mathbf{e} and \mathbf{b} are *emergent* electric and magnetic fields (see SM for our choice of electromagnetic units [17]).

A tantalizing modification to the Maxwell Lagrangian that has been entertained both in high energy as well as condensed matter physics is the introduction of the topological axion term $\mathcal{L}_{\varphi\gamma} = \alpha\varphi(\mathbf{e}\cdot\mathbf{b})/\pi$ [18], where $\alpha = e^2/(4\pi c)$ is the fine structure constant¹ [19] and φ is a real pseudoscalar called the axion field. In high-energy physics, axions are considered one of the best motivated particles beyond the standard model, acting as a remedy to the strong CP problem [20], naturally arising in string theory [21], and playing a role as a possible dark-matter candidate [22]. Despite decades of intensive experimental efforts, such axions have not been observed [23].

Axions can also emerge as collective excitations in condensed matter systems [18, 24]. Indeed, the fluctuations of any (anti)ferromagnetic ordering with a pseudoscalar order parameter couple as a dynamical axion field at long wavelengths. In the context of topological insulators, a spacetime constant φ (in which case, the axion term is called a θ term in the literature) plays an important role in the electromagnetic response [25–27], and the influence of dynamical axionic fluctuations on the external electromagnetic fields has been studied in considerable detail [28–31]. Additionally, they have been discussed in the context of topological superconductors [32] as well as Weyl semimetals [33, 34].

Here we investigate the effects of an emergent dynamical axion in $U(1)$ QSLs. This scenario has received limited attention in the literature and remains poorly understood beyond some work on the effect of θ -terms [35–38]. The dynamical axion we study couples directly to the external electromagnetic field, like the axions in topological insulators. Importantly, however, it also couples to the emergent electrodynamics, giving rise to a vacuum with elementary photons and axions that has been hitherto inaccessible in other contexts. We study this internal axion electrodynamics by investigating the dynamical structure factor, and we show how it leads to prominent signatures that can be accessed through inelastic neutron scattering. Namely, we find a characteristic two-particle continuum associated with the threshold production of axion-photon pairs. We further discuss possible experimental realizations in quantum spin ice on the breathing pyrochlore lattice, where an appropriate magnetic order interacts with the emergent gauge field as an axion field, see Fig. 1. This identifies breathing pyrochlore QSL candidates, like $\text{Ba}_3\text{Yb}_2\text{Zn}_5\text{O}_{11}$ [40], as a possible condensed-matter realization of emergent axion electrodynamics.

Low-energy effective action — $U(1)$ QSLs are described by the deconfined phase of a compact abelian lattice gauge theory [41]. This is well established in microscopic models of spins dominated by ring-exchange interactions [6, 42–44]. However, regularizing the axion

¹ Here c is the ‘speed of light’ and e is the elementary ‘electric charge’, both associated with the emergent gauge structure.

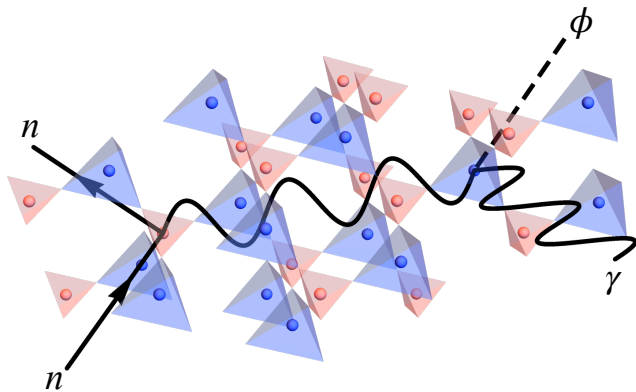


FIG. 1. In the breathing pyrochlore lattice, the A (red) and B (blue) tetrahedra have different volume, breaking inversion symmetry. A staggered spinon charge density, with positive (red sphere) and negative (blue sphere) spinons on A and B tetrahedra, respectively, breaks time reversal [39]. The combined order couples as an axion to the internal electrodynamics. The embedded Feynman diagram illustrates one of the neutron scattering processes brought about by the possibility of photon-axion pair production.

term on the lattice generally involves complicated, beyond nearest-neighbour interactions [45–48].

Here we proceed by coarse-graining the microscopic degrees of freedom and writing down the leading symmetry-allowed terms in a long-wavelength effective action. We separate the axion field into a vacuum expectation value and fluctuations: $\varphi(\mathbf{x}, t) \equiv \theta + \phi(\mathbf{x}, t)$. This leads to the low-energy effective action $S_{\text{eff}} = \int d^3\mathbf{x} dt \{ \mathcal{L}_\gamma + \mathcal{L}_\phi + \mathcal{L}_{\varphi\gamma} \}$ in Minkowski spacetime, where

$$\mathcal{L}_\gamma = \frac{1}{2} (|\mathbf{e}|^2 - |\mathbf{b}|^2), \quad (1a)$$

$$\mathcal{L}_\phi = \frac{J}{2} \left((\partial_t \phi)^2 - v^2 |\nabla \phi|^2 - \Delta^2 \phi^2 \right), \quad (1b)$$

$$\mathcal{L}_{\varphi\gamma} = \frac{\alpha}{\pi} (\theta + \phi) \mathbf{e} \cdot \mathbf{b}. \quad (1c)$$

\mathcal{L}_γ and $\mathcal{L}_{\varphi\gamma}$ are the aforementioned Maxwell Lagrangian and axion contributions, where $\alpha \sim 1/10$ is the emergent fine structure constant [19], governing the emergent electric and magnetic fields $\mathbf{e}(\mathbf{x}, t)$ and $\mathbf{b}(\mathbf{x}, t)$. \mathcal{L}_ϕ is the free theory for the emergent axion, where the phenomenological parameters J , v , and Δ correspond to the axion's stiffness, asymptotic speed, and gap, respectively. Except when $v = c$, the emergent speed of light, the axion sector of the theory violates the emergent Lorentz invariance. In this work, we do not consider contributions in S_{eff} from the gapped electric gauge charges (spinons) and magnetic monopoles (visons). Furthermore, S_{eff} could include additional terms with real background electric and magnetic fields $\mathbf{E}(\mathbf{x}, t)$ and $\mathbf{B}(\mathbf{x}, t)$ interacting with the emergent axion field φ (i.e., $\mathcal{L}_{\text{ext}} \sim \varphi \mathbf{E} \cdot \mathbf{B}$) as in topological insulators [28–31]. Here, we focus on how the axion interacts with the emergent electromagnetic fields,

Eq. (1c), as this physics is new to the QSL context. We return briefly to the coupling to external electromagnetic fields at the end of this letter.

It is well known that the θ -term is a total derivative and does not affect the dynamical equations of motion in the bulk. However, the presence of the axion term modifies the emergent Gauss's law as a Gauss-Witten law [49]

$$\nabla \cdot \mathbf{e} = -\frac{\alpha}{\pi} \nabla \cdot (\varphi \mathbf{b}). \quad (2)$$

This reveals the Witten effect, where the axion field causes magnetic monopoles to accumulate fractional electric charge [50]. For our purposes, it will also be important in identifying the degrees of freedom to which external probe-fields couple.

Axions in quantum spin ice — Before turning to our results on the dynamics of axion-photon production, we contextualize them to the case of quantum spin ice (QSI) systems. This is both because QSI has become a familiar model system for $U(1)$ QSLs [6–8], and also because of its direct experimental relevance, with several candidate materials under current investigation [9–15].

In the first instance, we need to identify an experimentally motivated order parameter, φ , that interacts with the emergent photon as an axion. To be consistent with the field-theoretic modeling above, upon coarse-graining, φ must be a local time-reversal odd pseudoscalar in order to linearly couple with $\mathbf{e} \cdot \mathbf{b}$.

It is tempting to consider a common magnetic order parameter in pyrochlore systems [51], namely

$$Q_t = (-1)^t \text{div}_t S^{(z)}. \quad (3)$$

Here, t labels tetrahedra on the pyrochlore lattice and $(-1)^t = \pm 1$ depending on the sublattice (A or B). $\text{div}_t S^{(z)}$ is the lattice divergence of $S^{(z)}$ — the component of the spin along the local easy axis — which yields the spinon charge at t . Evidently, Q_t is an order parameter for a staggered background of spinons, which corresponds to the spins developing all-in-all-out order and spontaneously breaking time-reversal symmetry [39]. However, this real order parameter is even under inversion and does not have the correct symmetry properties.

We are therefore brought to consider the breathing pyrochlore lattice, shown in Fig. 1, where A and B tetrahedra are of unequal size and thus no longer relate under inversion. For small enough breathing anisotropy, the $U(1)$ QSL phase of QSI remains stable [52]. The breathing anisotropy only modifies the microscopic ring-exchange scale, which changes the value of the internal speed of light but does not affect the stability of the effective field theory.

The breathing anisotropy is characterized by the lattice order parameter

$$\Delta V_l = a^{-3} \left(V_l^{(A)} - V_l^{(B)} \right), \quad (4)$$

where, $V_l^{(A)}$ ($V_l^{(B)}$) is the volume of the A (B) tetrahedron with corner at site l , and a is the lattice constant.

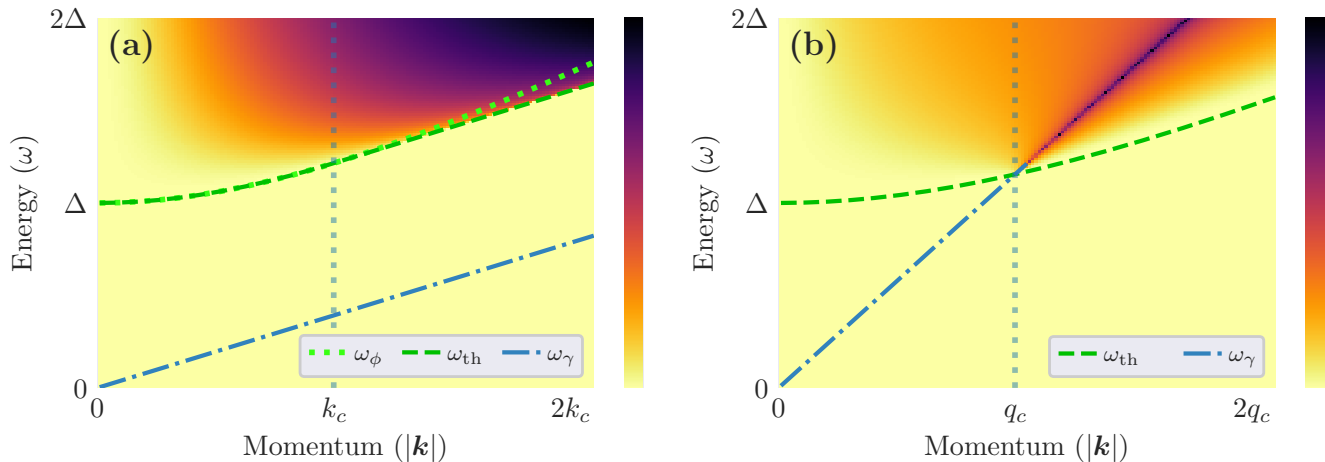


FIG. 2. The dynamical structure factor $\mathcal{F}^{aa}(\mathbf{k}, \omega)$ exhibits a two-particle continuum due to axion-photon pair production above a threshold ω_{th} (green dashed line, see Eq. (7)). Below threshold, the delta function response due to single photon states is indicated by ω_{γ} (blue dash-dotted line). Depending on the kinematics of the axion dispersion, either the axion can travel faster than the speed of light (a) or not (b). In the former case, the critical momentum beyond which the axion would travel faster than the speed of light is k_c . In the latter case, the single-photon dispersion enters the photon-axion continuum above total momentum q_c , leading to a resonance centered at ω_{γ} (vertical dotted lines in the respective panels).

Evidently, ΔV is a time-reversal even real pseudoscalar, and the product $Q\Delta V$ finally has the correct symmetry. Coarse-graining and decomposing the order parameters into their vacuum expectation values and amplitude fluctuations, we obtain an axion field

$$\varphi(\mathbf{x}, t) \equiv \theta + \phi(\mathbf{x}, t) \sim \langle \Delta V \rangle \langle Q \rangle + \langle \Delta V \rangle \delta Q(\mathbf{x}, t). \quad (5)$$

Here we have neglected fluctuations of ΔV as we generally expect lattice distortions to have higher energy than the magnetic fluctuations.

Axion-photon production — In order to probe the coupled dynamics of the axion-photon system, we study the dynamical structure factor (DSF) of the coarse-grained spin magnetic moment $\mathbf{S}(\mathbf{x}, t)$. This can be measured by neutron scattering and is often used to probe candidate spin liquids [9, 12, 14, 15, 53]. The DSF $\mathcal{F}^{ij}(\mathbf{k}, \omega)$ is given by the imaginary part of the spin susceptibility associated with the correlation function $\langle S^i(\mathbf{k}, \omega) S^j(-\mathbf{k}, -\omega) \rangle$, where $i, j = x, y, z$.

The most interesting contribution to the DSF within the low-energy effective theory, Eq. (1), is due to the threshold production of axion-photon pairs. While we do not model spinon-axion interactions, we note that they could modify the DSF in the spin-flip channel and cause an additional multi-particle continuum [54, 55].

To compute the DSF, we must connect $\mathbf{S}(\mathbf{x}, t)$ to the degrees of freedom present in the effective field theory. Below the spinon gap, physical states satisfy the divergence-free condition $\nabla \cdot \mathbf{S} = 0$. Comparing this to the Gauss-Witten law of our theory, Eq. (2), up to a non-universal constant, $\mathbf{S}(\mathbf{x}, t)$ is therefore given by

$$\mathbf{S}(\mathbf{x}, t) = \mathbf{e}(\mathbf{x}, t) + \frac{\alpha}{\pi} \varphi(\mathbf{x}, t) \mathbf{b}(\mathbf{x}, t). \quad (6)$$

Eq. (6) can be further confirmed by noting that on the lattice the emergent vector potential and spin magnetic moment are canonically conjugate [6, 56, 57]. Identifying the coarse-grained $\mathbf{S}(\mathbf{x}, t)$ as the canonical momentum of the effective field theory, the variation $\delta S_{\text{eff}}/\delta \mathbf{e}$ once again yields Eq. (6).

With this identification, the DSF $\mathcal{F}^{ij}(\mathbf{k}, \omega)$ must be transverse. Solving the Schwinger-Dyson equation to leading loop order, we find (see SM [17]),

$$\mathcal{F}^{ij} = \left(\delta^{ij} - \frac{k^i k^j}{k^2} \right) \begin{cases} \mathcal{F}_{\gamma}(\mathbf{k}, \omega) \delta(\omega - c|\mathbf{k}|) & \omega < \omega_{\text{th}}(\mathbf{k}) \\ \mathcal{F}_{\phi\gamma}(\mathbf{k}, \omega) & \omega > \omega_{\text{th}}(\mathbf{k}). \end{cases} \quad (7)$$

Here, ω_{th} indicates the threshold energy above which axion-photon pairs can be produced at total momentum \mathbf{k} . The associated two-particle continuum is represented by $\mathcal{F}_{\phi\gamma}$, which in the absence of the emergent axion vanishes. Below the threshold, only single photon states are available and the DSF contains a delta function reflecting the photon dispersion, weighted by the function $\mathcal{F}_{\gamma} = (\pi + \alpha^2 \theta^2 / \pi) \omega$. This reduces to the well known result for standard $U(1)$ QSLs when $\theta = 0$ [56, 58].

In general, the effective theory is not Lorentz invariant unless the asymptotic velocity of the axion field, v , equals the speed of light, c . Thus, there are two distinct kinematic regimes for axion-photon production corresponding to $v \geq c$ and $v < c$, as illustrated in Fig. 2(a) and (b) respectively. In the case $v \geq c$, there is a critical momentum $k_c = \Delta c / (v\sqrt{v^2 - c^2})$ beyond which the axion travels faster than c . This leads to the threshold

$$\omega_{\text{th}} = \begin{cases} \omega_{\phi}(\mathbf{k}) & |\mathbf{k}| < k_c \\ \omega_{\gamma}(|\mathbf{k}| - k_c) + \omega_{\phi}(k_c) & |\mathbf{k}| \geq k_c \end{cases}, \quad (8)$$

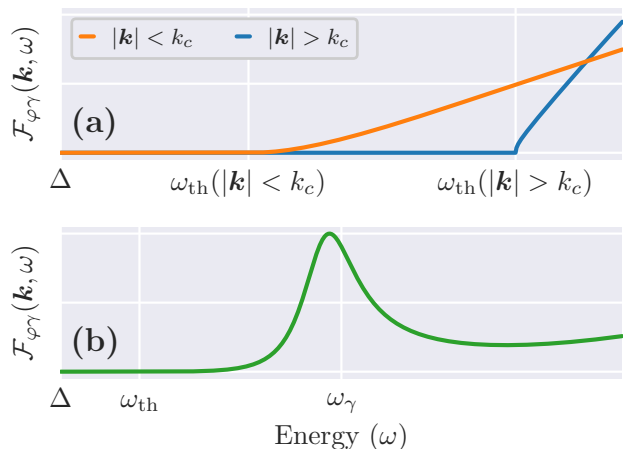


FIG. 3. Line cuts of the dynamical structure factor $\mathcal{F}_{\phi\gamma}(\mathbf{k}, \omega)$ at fixed momentum $|\mathbf{k}|$ illustrating, for different kinematic regimes, (a) the turn on of the axion-photon continuum above threshold and (b) the single photon resonance on top of the continuum. For convenience, we have chosen parameters that produce a broad resonance with visible Fano asymmetry on the scale of the background.

where $\omega_\phi(|\mathbf{k}|) = \sqrt{\Delta^2 + v^2|\mathbf{k}|^2}$ and $\omega_\gamma(|\mathbf{k}|) = c|\mathbf{k}|$ are the axion and photon dispersions, respectively. Physically, for external momenta less than k_c , all of the momentum is carried by the axion at threshold. For greater momenta, the axion travels at c and the rest of the momentum is carried by the photon. While the full functional form of $\mathcal{F}_{\phi\gamma}$ is cumbersome (see SM [17]), the behavior just above threshold is governed by characteristic exponents,

$$\mathcal{F}_{\phi\gamma}(\mathbf{k}, \omega) \sim \begin{cases} (\omega - \omega_{\text{th}})^3 & |\mathbf{k}| \leq k_c \\ \sqrt{\omega - \omega_{\text{th}}} & |\mathbf{k}| > k_c \end{cases}. \quad (9)$$

See Fig. 3(a) for frequency dependent line cuts of the full DSF illustrating these two behaviors. Notice that the naive expectation, based on the density of axion-photon states, goes as $(\omega - \omega_{\text{th}})^2$ for $|\mathbf{k}| < k_c$ and $\sqrt{\omega - \omega_{\text{th}}}$ for $|\mathbf{k}| > k_c$. The difference can be traced to the momentum dependence of the interaction.

In the case that $v < c$, the axion never reaches the speed of light so $\omega_{\text{th}} = \omega_\phi$. However, the single-photon dispersion crosses above ω_{th} for momenta greater than $q_c = \Delta/\sqrt{c^2 - v^2}$. In this regime, a single photon can decay into an axion-photon pair and the DSF develops a resonant peak above threshold, see Fig. 3(b). The Fano-like asymmetry [59] of the resonant line-shape can be traced to the interference between the \mathbf{e} operator in Eq. (6) creating a single-photon state which decays into an axion-photon pair and the $\varphi\mathbf{b}$ operator directly producing such a pair.

The experimental signatures of the axion discussed thus far are due to interactions with photons. It is interesting to consider whether a dynamical axion field can be

detected through inelastic neutron scattering in the absence of an emergent electrodynamics. In this case, there are no long-wavelength pseudovectors at the Γ point to couple to the neutron spin. Returning to the example of breathing pyrochlore, this indicates that fluctuations of Q remain hidden to neutrons unless there is coexisting $U(1)$ fractionalization.

Coupling to external electromagnetic fields — On symmetry grounds alone, the order parameter $\phi \sim Q\Delta V$ couples to the external electromagnetic field as well, leading to a magneto-electric polarizability in linear response. Since the charge gap is large in these materials, the response of the conduction and valence bands to the magnetic ordering should be weak [25], producing a small electronic contribution to the response. Rather, we expect a significant contribution would rely on the Khomskii polarization mechanism [60], wherein an electric dipole moment arises in tetrahedra that host spinon excitations pointing in the direction of the minority spin. In non-breathing pyrochlores, this cancels for adjacent spinon-antispinon pairs; with breathing, it need not. In the absence of an applied magnetic field, the staggered Q order parameter corresponds to a spinon-antispinon (salt-like) crystal with no preferred orientation for the minority spins, and the associated Khomskii polarization cancels. An applied magnetic field would make certain spins preferentially ‘minority’ for the existing salt crystal, which in turn leads to a linear electric polarization. A quantitative study of this microscopic mechanism is beyond the scope of the present paper.

Discussion — We studied the dynamical interplay of axion and gauge fields in the context of quantum spin liquids (QSL), where they both appear as emergent phenomena. We identified a microscopic order parameter that has the right symmetry to give rise to an emergent axion field. This order is natural in quantum spin ice systems on breathing pyrochlore lattices [52], such as the QSL candidate $\text{Ba}_3\text{Yb}_2\text{Zn}_5\text{O}_{11}$ [40, 61–63]. The two main ingredients are the breaking of lattice inversion symmetry coexisting with low energy fluctuations of a scalar antiferromagnetic order parameter Q . From Eq. (5), a finite θ parameter requires $\langle Q \rangle \neq 0$. Classically, such order can coexist with Coulomb liquid behavior, for example, in the fragmented phase of spin ice [64, 65], which has been recently observed in iridate materials [66–68]. Our long-wavelength symmetry analysis suggests that the quantum limit of a fragmented spin liquid on breathing pyrochlore would be a $U(1)$ QSL phase with both a θ -term and a dynamical axion. Notice, however, that the dynamical part of the axion, ϕ , comes from the amplitude fluctuations of Q , and is therefore present regardless of $\langle Q \rangle$.

Unlike the axion electrodynamics studied in topological insulators and superconductors, and in Weyl semimetals [28–30, 32–34], the quasiparticle content of $U(1)$ QSLs includes magnetic monopoles. In the presence of a finite θ -term, the celebrated Witten effect induces the monopoles to acquire an electric charge, becoming dyons,

which in turn leads to possible changes in the thermodynamic behavior of the system. For instance, condensation of dyons (called oblique confinement [45]) can lead to distinct symmetry patterns in the neighboring ordered phases [36].

Here, we focused instead on a dynamical axion, which modifies the inelastic response and may be observed directly in neutron scattering. Using a long-wavelength description, we investigated the behavior of the dynamical structure factor and demonstrated how it is qualitatively modified by the axion-photon continuum, as shown in Fig. 2. Our results provide an avenue to observe signatures of emergent axion electrodynamics in a class of frustrated magnetic systems. These signatures crucially depend on the presence of the underlying $U(1)$ gauge structure and therefore also provide direct evidence of QSL behavior.

Dynamical axions in our universe were first hypothesized over 40 years ago as a remedy for the strong CP problem in the standard model [69]. Today they are the subject of intense experimental searches as strong candidates for dark matter [22], yet to be observed [23]. In

condensed matter systems, while pseudoscalar collective modes are not so elusive, their coupling to a fully internal electrodynamics is not readily available. In this paper, we demonstrated how one can realize and access an emergent axion electrodynamics in the context of quantum spin liquids. Speculatively, this provides a test bed for high-energy physics that cannot be currently probed directly due to limitations of experiments or, more dramatically, limitations in the content of the universe itself.

Acknowledgements — The authors are grateful to Anushya Chandran, Pieter Claeys, Michael DeMarco, Eduardo Fradkin, Joseph Maciejko, Siddhardh Morampudi, and David Tong for useful discussions. S.D.P. acknowledges support from The Winston Churchill Foundation of the United States through the Churchill Scholarship, and support from the Henry W. Kendall Fellowship. This work was supported in part by the Engineering and Physical Sciences Research Council (EPSRC) under grants EP/M007065/1, EP/P034616/1 and EP/T028580/1 (C.C. and S.D.P.). C.R.L. acknowledges support from the NSF through grant PHY-1752727 and the generous hospitality of the Aspen Center for Physics, which is supported by NSF grant PHY-1607611.

-
- [1] P. W. Anderson, *Science* **235**, 1196 (1987).
 [2] L. Savary and L. Balents, *Rep. Prog. Phys.* **80**, 016502 (2016).
 [3] Y. Zhou, K. Kanoda, and T.-K. Ng, *Rev. Mod. Phys.* **89**, 025003 (2017).
 [4] M. Levin and X.-G. Wen, *Rev. Mod. Phys.* **77**, 871 (2005).
 [5] C. L. Henley, *Annu. Rev. Condens. Matter Phys.* **1**, 179 (2010).
 [6] M. Hermele, M. P. Fisher, and L. Balents, *Phys. Rev. B* **69**, 064404 (2004).
 [7] N. Shannon, O. Sikora, F. Pollmann, K. Penc, and P. Fulde, *Phys. Rev. Lett.* **108**, 067204 (2012).
 [8] M. J. Gingras and P. A. McClarty, *Rep. Prog. Phys.* **77**, 056501 (2014).
 [9] K. A. Ross, L. Savary, B. D. Gaulin, and L. Balents, *Phys. Rev. X* **1**, 021002 (2011).
 [10] R. Sibille, E. Lhotel, V. Pomjakushin, C. Baines, T. Fennell, and M. Kenzelmann, *Phys. Rev. Lett.* **115**, 097202 (2015).
 [11] L. Pan, N. Laurita, K. A. Ross, B. D. Gaulin, and N. Armitage, *Nat. Phys.* **12**, 361 (2016).
 [12] V. K. Anand, L. Opherden, J. Xu, D. T. Adroja, A. T. M. N. Islam, T. Herrmannsdörfer, J. Hornung, R. Schönemann, M. Uhlarz, H. C. Walker, N. Casati, and B. Lake, *Phys. Rev. B* **94**, 144415 (2016).
 [13] R. Sibille, N. Gauthier, H. Yan, M. C. Hatnean, J. Ollivier, B. Winn, U. Filges, G. Balakrishnan, M. Kenzelmann, N. Shannon, *et al.*, *Nat. Phys.* **14**, 711 (2018).
 [14] J. Gaudet, E. Smith, J. Dudemaine, J. Beare, C. Buhariwalla, N. P. Butch, M. Stone, A. Kolesnikov, G. Xu, D. Yahne, *et al.*, *Phys. Rev. Lett.* **122**, 187201 (2019).
 [15] B. Gao, T. Chen, D. W. Tam, C.-L. Huang, K. Sasmal, D. T. Adroja, F. Ye, H. Cao, G. Sala, M. B. Stone, *et al.*, *Nat. Phys.* **15**, 1052 (2019).
 [16] The terminology for $U(1)$ QSL excitations differs among communities. We denote the spinon as the electric gauge charge, sourcing *emergent* electric fields. Spinons are referred to as magnetic monopoles in the spin ice literature, as they source *real* magnetization fields. The excitations we call magnetic monopoles source *emergent* magnetic fields and undergo the Witten effect. In spin ice, they are often referred to as visons.
 [17] See Supplementary Material (appended) for a discussion of (i) the electromagnetic units used throughout the manuscript, (ii) the local easy axes of the (breathing) pyrochlore lattice in quantum spin ice, (iii) the symmetry properties of the emergent gauge field and axion, and (iv) the calculation of the dynamical structure factor.
 [18] F. Wilczek, *Phys. Rev. Lett.* **58**, 1799 (1987).
 [19] S. D. Pace, S. C. Morampudi, R. Moessner, and C. R. Laumann, *Phys. Rev. Lett.* **127**, 117205 (2021).
 [20] J. E. Kim and G. Carosi, *Rev. Mod. Phys.* **82**, 557 (2010).
 [21] P. Svrcek and E. Witten, *J. High Energy Phys.* **2006**, 051 (2006).
 [22] L. D. Duffy and K. Van Bibber, *New J. Phys.* **11**, 105008 (2009).
 [23] P. W. Graham, I. G. Irastorza, S. K. Lamoreaux, A. Lindner, and K. A. van Bibber, *Annu. Rev. Nucl. Part. Sci.* **65**, 485 (2015).
 [24] P. W. Anderson, *Science* **177**, 393 (1972).
 [25] X.-L. Qi, T. L. Hughes, and S.-C. Zhang, *Phys. Rev. B* **78**, 195424 (2008).
 [26] G. Y. Cho and J. E. Moore, *Ann. Phys. (N. Y.)* **326**, 1515 (2011).
 [27] A. Chan, T. L. Hughes, S. Ryu, and E. Fradkin, *Physical Review B* **87**, 085132 (2013).
 [28] R. Li, J. Wang, X.-L. Qi, and S.-C. Zhang, *Nat. Phys.*

- 6**, 284 (2010).
- [29] L. Wu, M. Salehi, N. Koirala, J. Moon, S. Oh, and N. Armitage, *Science* **354**, 1124 (2016).
- [30] D. M. Nenno, C. A. Garcia, J. Gooth, C. Felser, and P. Narang, *Nat. Rev. Phys.*, 1 (2020).
- [31] A. Sekine and K. Nomura, *J. Appl. Phys.* **129**, 141101 (2021).
- [32] X.-L. Qi, E. Witten, and S.-C. Zhang, *Phys. Rev. B* **87**, 134519 (2013).
- [33] Z. Wang and S.-C. Zhang, *Phys. Rev. B* **87**, 161107 (2013).
- [34] J. Gooth, B. Bradlyn, S. Honnali, C. Schindler, N. Kumar, J. Noky, Y. Qi, C. Shekhar, Y. Sun, Z. Wang, *et al.*, *Nature* **575**, 315 (2019).
- [35] D. Pesin and L. Balents, *Nat. Phys.* **6**, 376 (2010).
- [36] G. Y. Cho, C. Xu, J. E. Moore, and Y. B. Kim, *New J. Phys.* **14**, 115030 (2012).
- [37] C. Wang and T. Senthil, *Phys. Rev. X* **6**, 011034 (2016).
- [38] M. Pretko, *Phys. Rev. B* **96**, 125151 (2017).
- [39] On the pyrochlore lattice, all-out-all-in order ($Q \neq 0$) either has all spins on A tetrahedra pointing outwards while all spins on B tetrahedra point inwards, or vice versa. Unlike the more familiar Néel order on a square lattice, translation by primitive lattice vectors does not reverse the all-in-all-out order and time reversal symmetry cannot be restored by such a proper transformation. There is a space group symmetry which flips Q : mirror reflection (\mathcal{M}). However, \mathcal{M} involves a large, improper, transformation of space and it does not coarse-grain trivially. The combination of \mathcal{M} with time reversal is in fact a symmetry of the microscopic system which is consistent with the theta term in the continuum.
- [40] K. Kimura, S. Nakatsuji, and T. Kimura, *Phys. Rev. B* **90**, 060414 (2014).
- [41] S. Chandrasekharan and U.-J. Wiese, *Nucl. Phys. B* **492**, 455 (1997).
- [42] X.-G. Wen, *Phys. Rev. Lett.* **88**, 011602 (2001).
- [43] O. I. Motrunich and T. Senthil, *Phys. Rev. Lett.* **89**, 277004 (2002).
- [44] R. Moessner and S. L. Sondhi, *Phys. Rev. B* **68**, 184512 (2003).
- [45] J. L. Cardy and E. Rabinovici, *Nucl. Phys. B* **205**, 1 (1982).
- [46] D. G. Figueroa and M. Shaposhnikov, *Nucl. Phys. B* **926**, 544 (2018).
- [47] T. Sulejmanpasic and C. Gatteringer, *Nucl. Phys. B* **943**, 114616 (2019).
- [48] S. D. Pace and X.-G. Wen, *arXiv:2207.03544* (2022).
- [49] W. Fischler and J. Preskill, *Phys. Lett. B* **125**, 165 (1983).
- [50] E. Witten, *Phys. Lett. B* **86**, 283 (1979).
- [51] C. Castelnovo, R. Moessner, and S. L. Sondhi, *Annu. Rev. Condens. Matter Phys.* **3**, 35 (2012).
- [52] L. Savary, X. Wang, H.-Y. Kee, Y. B. Kim, Y. Yu, and G. Chen, *Phys. Rev. B* **94**, 075146 (2016).
- [53] J. Knolle and R. Moessner, *Annu. Rev. Condens. Matter Phys.* **10**, 451 (2019).
- [54] C.-J. Huang, Y. Deng, Y. Wan, and Z. Y. Meng, *Phys. Rev. Lett.* **120**, 167202 (2018).
- [55] S. C. Morampudi, F. Wilczek, and C. R. Laumann, *Phys. Rev. Lett.* **124**, 097204 (2020).
- [56] L. Savary and L. Balents, *Phys. Rev. Lett.* **108**, 037202 (2012).
- [57] M. Kwasigroch, B. Douçot, and C. Castelnovo, *Phys. Rev. B* **95**, 134439 (2017).
- [58] O. Benton, O. Sikora, and N. Shannon, *Phys. Rev. B* **86**, 075154 (2012).
- [59] U. Fano, *Phys. Rev.* **124**, 1866 (1961).
- [60] D. Khomskii, *Nature Communications* **3**, 904 (2012).
- [61] T. Haku, K. Kimura, Y. Matsumoto, M. Soda, M. Sera, D. Yu, R. A. Mole, T. Takeuchi, S. Nakatsuji, Y. Kono, T. Sakakibara, L.-J. Chang, and T. Masuda, *Phys. Rev. B* **93**, 220407 (2016).
- [62] J. G. Rau, L. S. Wu, A. F. May, L. Poudel, B. Winn, V. O. Garlea, A. Huq, P. Whitfield, A. E. Taylor, M. D. Lumsden, M. J. P. Gingras, and A. D. Christianson, *Phys. Rev. Lett.* **116**, 257204 (2016).
- [63] J. G. Rau and M. J. P. Gingras, *Phys. Rev. B* **98**, 054408 (2018).
- [64] M. Brooks-Bartlett, S. T. Banks, L. D. Jaubert, A. Harman-Clarke, and P. C. Holdsworth, *Phys. Rev. X* **4**, 011007 (2014).
- [65] E. Lhotel, L. D. Jaubert, and P. C. Holdsworth, *J. Low Temp. Phys.*, 1 (2020).
- [66] E. Lefrançois, V. Cathelin, E. Lhotel, J. Robert, P. Lejay, C. V. Colin, B. Canals, F. Damay, J. Ollivier, B. Fåk, *et al.*, *Nat. Commun.* **8**, 1 (2017).
- [67] V. Cathelin, E. Lefrançois, J. Robert, P. C. Guruciaga, C. Paulsen, D. Prabhakaran, P. Lejay, F. Damay, J. Ollivier, B. Fåk, L. C. Chapon, R. Ballou, V. Simonet, P. C. W. Holdsworth, and E. Lhotel, *Phys. Rev. Res.* **2**, 032073 (2020).
- [68] M. Pearce, K. Götze, A. Szabó, T. Sikkenk, M. Lees, A. Boothroyd, D. Prabhakaran, C. Castelnovo, and P. Goddard, *Nat. Commun* **13**, 1 (2022).
- [69] R. D. Peccei and H. R. Quinn, *Phys. Rev. Lett.* **38**, 1440 (1977).
- [70] L. Page, *Physics* **2**, 289 (1932).
- [71] J. G. Rau and M. J. Gingras, *Annu. Rev. Condens. Matter Phys.* (2019).

I. SUPPLEMENTAL MATERIAL

II. ELECTROMAGNETIC UNITS

Here we briefly explain the choice of electromagnetic units in the main text. For reference, in SI units the Maxwell Lagrangian is given by

$$\frac{\epsilon}{2}|\mathbf{e}_{\text{SI}}|^2 - \frac{1}{2\mu}|\mathbf{b}_{\text{SI}}|^2 \quad (10)$$

where ϵ and μ are the effective dielectric constant and magnetic permeability, respectively. The emergent speed of light c follows the standard relationship $c = 1/\sqrt{\epsilon\mu}$.

We work in Heaviside-Lorentz units [70], a type of CGS units where $\epsilon_0 = 1$ and the magnetic field is divided by c so \mathbf{e} and \mathbf{b} have the same units. In these units, the Maxwell Lagrangian is indeed

$$\mathcal{L}_\gamma = \frac{1}{2}|\mathbf{e}|^2 - \frac{1}{2}|\mathbf{b}|^2. \quad (11)$$

The electric field emitted from an electric charge, with charge e , is

$$\mathbf{e} = \frac{e}{4\pi|\mathbf{x}|^2}\hat{\mathbf{r}}, \quad (12)$$

and the magnetic field from a magnetic monopole, where g is its magnetic charge, is

$$\mathbf{b} = \frac{g}{4\pi c|\mathbf{x}|^2}\hat{\mathbf{r}}. \quad (13)$$

Futhermore, working with $\hbar = 1$, in these units the fine structure constant is given by

$$\alpha = \frac{e^2}{4\pi c}, \quad (14)$$

and Dirac's quantization is

$$\frac{eg}{c^2} = 2\pi n, \quad (15)$$

where $n \in \mathbb{Z}$. Finally, we note that the emergent gauge field is $a^\mu = (a^0, \mathbf{a})$, where a^0 is the electrostatic potential and \mathbf{a} the vector potential. The electric and magnetic fields, in terms of a^0 and \mathbf{a} , are

$$\mathbf{e} = -\nabla a^0 - \frac{1}{c}\partial_t \mathbf{a}, \quad (16)$$

$$\mathbf{b} = \nabla \times \mathbf{a}, \quad (17)$$

where we do not include magnetic monopole contributions in \mathbf{b} (see Eq. (27) further below).

III. (BREATHING) PYROCHLORE LATTICE AND LOCAL EASY AXES

The pyrochlore lattice is a network of corner-sharing tetrahedra that form a bipartite (diamond) lattice, as illustrated in Fig. 4(a) where sublattice A and B are shown in red and green, respectively. In pyrochlore magnets, spin degrees of freedom reside on the corners of the tetrahedra, and in spin ice they are restricted to point directly into or out of each tetrahedron. Because of the easy-axis (Ising) anisotropy, the spin operators are most conveniently defined in a local frame where a positive z -component of a spin points towards the center of a B tetrahedron, along the local $[1, 1, 1]$ direction. Indeed, consider an A tetrahedron centered at \mathbf{x} , whose four corners are labelled by $n = 1, 2, 3, 4$. In terms of the local frame, the spin vector $\boldsymbol{\mu}$ is given by

$$\boldsymbol{\mu}(\mathbf{x}, n) = S_{\mathbf{x},n}^{(x)}\hat{\mathbf{a}}_n + S_{\mathbf{x},n}^{(y)}\hat{\mathbf{b}}_n + S_{\mathbf{x},n}^{(z)}\hat{\mathbf{e}}_n, \quad (18)$$

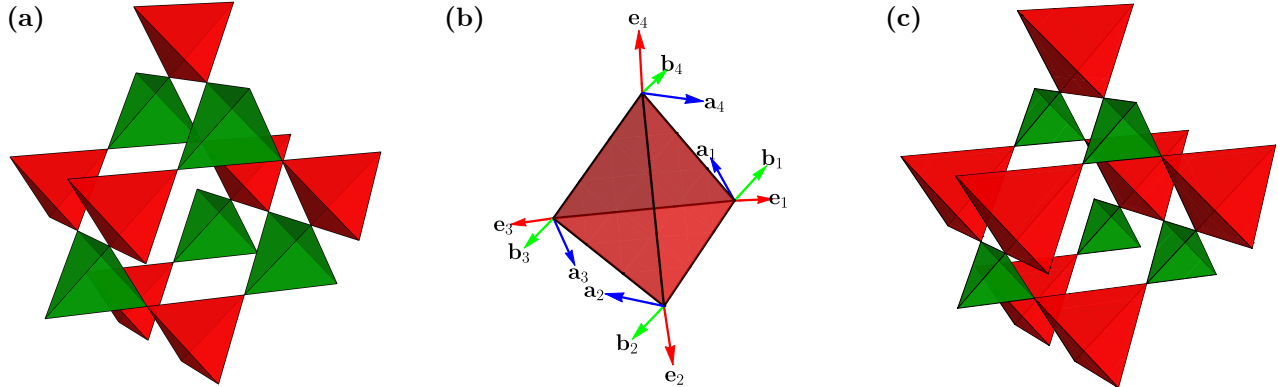


FIG. 4. The pyrochlore lattice is a prototypical setting for frustrated magnetism in $3 + 1D$. Panel (a) shows a chunk of the pyrochlore lattice with A tetrahedra colored in red and B tetrahedra in green. The four neighboring tetrahedra of an A (B) tetrahedron are all B (A) tetrahedra. Panel (b) shows an isolated A tetrahedron with the four conventional local axes shown for each corner. The $(\hat{\mathbf{a}}_n, \hat{\mathbf{b}}_n, \hat{\mathbf{e}}_n)$ vectors are defined in Eq. (19). (c) Breathing anisotropy refers to the A and B tetrahedra in the pyrochlore lattice becoming unequal in size. The breathing pyrochlore lattice — the pyrochlore lattice with breathing anisotropy — is shown, where the B tetrahedra have become smaller than A tetrahedra.

where the orthonormal vectors $(\hat{\mathbf{a}}_i, \hat{\mathbf{b}}_i, \hat{\mathbf{e}}_i)$ defining the local easy axes are given by [56]

$$\begin{aligned}
 \hat{\mathbf{a}}_1 &= \left(\frac{-2}{\sqrt{6}}, \frac{1}{\sqrt{6}}, \frac{1}{\sqrt{6}} \right), & \hat{\mathbf{b}}_1 &= \left(0, \frac{-1}{\sqrt{2}}, \frac{1}{\sqrt{2}} \right), & \hat{\mathbf{e}}_1 &= \left(\frac{1}{\sqrt{3}}, \frac{1}{\sqrt{3}}, \frac{1}{\sqrt{3}} \right), \\
 \hat{\mathbf{a}}_2 &= \left(\frac{-2}{\sqrt{6}}, \frac{-1}{\sqrt{6}}, \frac{-1}{\sqrt{6}} \right), & \hat{\mathbf{b}}_2 &= \left(0, \frac{1}{\sqrt{2}}, \frac{-1}{\sqrt{2}} \right), & \hat{\mathbf{e}}_2 &= \left(\frac{1}{\sqrt{3}}, \frac{-1}{\sqrt{3}}, \frac{-1}{\sqrt{3}} \right), \\
 \hat{\mathbf{a}}_3 &= \left(\frac{2}{\sqrt{6}}, \frac{1}{\sqrt{6}}, \frac{-1}{\sqrt{6}} \right), & \hat{\mathbf{b}}_3 &= \left(0, \frac{-1}{\sqrt{2}}, \frac{-1}{\sqrt{2}} \right), & \hat{\mathbf{e}}_3 &= \left(\frac{-1}{\sqrt{3}}, \frac{1}{\sqrt{3}}, \frac{-1}{\sqrt{3}} \right), \\
 \hat{\mathbf{a}}_4 &= \left(\frac{2}{\sqrt{6}}, \frac{-1}{\sqrt{6}}, \frac{1}{\sqrt{6}} \right), & \hat{\mathbf{b}}_4 &= \left(0, \frac{1}{\sqrt{2}}, \frac{1}{\sqrt{2}} \right), & \hat{\mathbf{e}}_4 &= \left(\frac{-1}{\sqrt{3}}, \frac{-1}{\sqrt{3}}, \frac{1}{\sqrt{3}} \right).
 \end{aligned} \tag{19}$$

An A tetrahedron with these four local coordinate systems is shown in Fig. 4(b). In the main text, we focused on the magnetic moment part of the total spin vector. For simplicity, we used a single index $l \equiv (\mathbf{x}, n)$ for the spin (pyrochlore) sites, and we further considered the coarse grained, continuum limit: $\mathbf{S}_l \rightarrow \mathbf{S}(\mathbf{x})$.

As discussed in this work, in order to realise an emergent axion electrodynamics, we need a breathing pyrochlore lattice. Under such anisotropy, the A and B tetrahedra are of unequal size and the inversion symmetry about a site is broken, which reduces the pyrochlore lattice space group, $Fd\bar{3}m$, down to $F\bar{4}3m$. Fig. 4(c) shows the breathing pyrochlore lattice with the A tetrahedra (in red) larger than the B tetrahedra (in green).

IV. SYMMETRY PROPERTIES OF THE EMERGENT FIELDS IN QUANTUM SPIN ICE

Here we discuss the symmetry properties of the emergent gauge field, a^μ , and axion field, ϕ , which in turn derive from the combined symmetry properties of the microscopic spin-1/2 moments and of the lattice. We consider quantum spin ice (QSI), where spins reside on the pyrochlore lattice (see Fig. 4), and follow the notation $S_l^{(z)} = 1/2$ for a spin at site i pointing into a B tetrahedron (and $S_l^{(z)} = -1/2$ for a spin pointing into an A tetrahedron).

We focus on spin-1/2 degrees of freedom realized by magnetic doublets with the following properties under time-reversal, \mathcal{T} , and inversion, \mathcal{I} , about a pyrochlore lattice site:

$$\mathcal{T}: S_l^{(z)}(t) \rightarrow -S_l^{(z)}(-t), \tag{20}$$

$$\mathcal{I}: \mathbf{S}_l(t) \rightarrow \mathbf{S}_{\mathcal{I}(l)}(t). \tag{21}$$

These properties are satisfied by Kramers, non-Kramers, and dipolar–octupolar doublets, which make up all of the possible magnetic doublets in QSI candidate materials [71]. They encompass the Kramers doublets carried by the Yb^{3+} ions in $\text{Ba}_3\text{Yb}_2\text{Zn}_5\text{O}_{11}$, which is the quantum breathing pyrochlore magnet discussed in the main text.

The emergent gauge potential on the lattice is canonically conjugate to $S^{(z)}$, thus satisfying $[a_l(t), S_l^{(z)}(t')] = i\delta_{ll'}\delta(t-t')$. We can use this canonical commutation relation to find the symmetry properties of $a_l(t)$. Requiring that $a_l(t)$ transforms in such a way that the commutation relations are left unchanged – up to a constant shift which can be removed by a gauge transformation – the emergent gauge potential transforms as

$$\mathcal{T}: a_l(t) \rightarrow a_l(-t), \quad (22)$$

$$\mathcal{I}: a_l(t) \rightarrow a_{\mathcal{I}(l)}(t). \quad (23)$$

For Eq. (22), we used that \mathcal{T} is an anti-unitary operator that changes the sign of the imaginary unit i in the commutation relation. From here, we can then connect the symmetry properties to the electric and magnetic field variables using the lattice definitions of the gradient and curl based on discrete differential forms. However, it is more convenient instead to first coarse-grain the vector potential and work with these differential operators in the continuum:

$$\mathcal{T}: \mathbf{a}(\mathbf{x}, t) \rightarrow \mathbf{a}(\mathbf{x}, -t), \quad (24)$$

$$\mathcal{I}: \mathbf{a}(\mathbf{x}, t) \rightarrow \mathbf{a}(-\mathbf{x}, t). \quad (25)$$

Taking into account that we have a compact gauge potential and thus magnetic monopoles, \mathbf{e} and \mathbf{b} are related to the emergent gauge field $a^\mu = (a^0, \mathbf{a})$ by the relationships

$$\mathbf{e} = -\nabla a^0 - \frac{1}{c}\partial_t \mathbf{a}, \quad (26)$$

$$\mathbf{b} = \nabla \times \mathbf{a} + \mathbf{n}, \quad (27)$$

where $\nabla \cdot \mathbf{n}$ equals the magnetic monopole magnetic charge g . From these definitions, we see that the electric field transforms like $\partial_t \mathbf{a}$ and the magnetic field transforms like $\nabla \times \mathbf{a}$. Therefore, under time-reversal the emergent electric and magnetic fields transform as

$$\mathcal{T}: \mathbf{e}(\mathbf{x}, t) \rightarrow -\mathbf{e}(\mathbf{x}, -t), \quad (28)$$

$$\mathcal{T}: \mathbf{b}(\mathbf{x}, t) \rightarrow \mathbf{b}(\mathbf{x}, -t), \quad (29)$$

and under inversion they transform as

$$\mathcal{I}: \mathbf{e}(\mathbf{x}, t) \rightarrow \mathbf{e}(-\mathbf{x}, t), \quad (30)$$

$$\mathcal{I}: \mathbf{b}(\mathbf{x}, t) \rightarrow -\mathbf{b}(-\mathbf{x}, t). \quad (31)$$

We see that the emergent electric and magnetic fields transform oppositely under \mathcal{T} and \mathcal{I} when we compare them to the external electric and magnetic fields. However, $\mathbf{e} \cdot \mathbf{b}$ transforms in the same way in both emergent and external electromagnetism. In fact, because $\mathbf{e} \cdot \mathbf{b}$ transforms like $(\partial_t \mathbf{a} \cdot \nabla \times \mathbf{a})$, it is always a time-reversal odd pseudoscalar, regardless of how the gauge field transforms. Additionally, we see that ∇a^0 transforms like \mathbf{e} and thus a^0 is time-reversal odd pseudoscalar.

From the symmetry properties of the emergent electric and magnetic fields, we find the symmetry properties of the electric and magnetic charge density, $\rho_e(\mathbf{x}, t)$ and $\rho_m(\mathbf{x}, t)$ respectively. Under time-reversal, these charge densities transform as

$$\mathcal{T}: \rho_e(\mathbf{x}, t) \rightarrow -\rho_e(\mathbf{x}, -t), \quad (32)$$

$$\mathcal{T}: \rho_m(\mathbf{x}, t) \rightarrow \rho_m(\mathbf{x}, -t), \quad (33)$$

and under inversion they transform as

$$\mathcal{I}: \rho_e(\mathbf{x}, t) \rightarrow -\rho_e(-\mathbf{x}, t), \quad (34)$$

$$\mathcal{I}: \rho_m(\mathbf{x}, t) \rightarrow \rho_m(-\mathbf{x}, t). \quad (35)$$

We see that $\rho_m(\mathbf{x}, t)$ is a time-reversal even scalar field while $\rho_e(\mathbf{x}, t)$ is a time-reversal odd pseudoscalar. One may note that $\rho_e(\mathbf{x}, t)$ has the required symmetry properties to interact with emergent photons as an emergent axion. However, because it is the divergence of a vector field, it fails to satisfy the requirement of having well-defined local

fluctuations that survive coarse-graining. As for other symmetries, the coarse-grained fields simply transform as vectors/pseudovectors or scalars/pseudoscalars.

We now discuss the symmetry properties of the order parameters Q and ΔV defined in Eq. (3) and (4), respectively, in the main text. The order parameter Q can be written in terms of $S^{(z)}$ using the definition of the lattice divergence

$$\text{div}_t S^{(z)} = (-1)^t \sum_{l \in t} S_l^{(z)}, \quad (36)$$

where the sum is over the pyrochlore lattice sites, l , making up the four corners of tetrahedron t . Plugging this into Eq. (3) yields

$$Q_t = \sum_{l \in t} S_l^{(z)}. \quad (37)$$

From the symmetry properties of $S^{(z)}$, it is straight-forward to see that Q transforms under \mathcal{T} and \mathcal{I} as

$$\mathcal{T}: Q_t(t) \rightarrow -Q_t(-t), \quad (38)$$

$$\mathcal{I}: Q_t(t) \rightarrow Q_{\mathcal{I}(t)}(t). \quad (39)$$

Using the fact that the lattice remains unchanged under \mathcal{T} , ΔV_l clearly transforms as

$$\mathcal{T}: \Delta V_l(t) \rightarrow \Delta V_l(-t). \quad (40)$$

As for inversion, because \mathcal{I} takes every A (B) tetrahedron to a B (A) tetrahedron, we have that

$$\mathcal{I}: \Delta V_l(t) \rightarrow -\Delta V_{\mathcal{I}(l)}(t). \quad (41)$$

Upon coarse-graining the order parameters, in the continuum limit the fields $Q(\mathbf{x}, t)$ and $\Delta V(\mathbf{x}, t)$ transform as

$$\mathcal{T}: Q(\mathbf{x}, t) \rightarrow -Q(\mathbf{x}, -t) \quad \Delta V(\mathbf{x}, t) \rightarrow \Delta V(\mathbf{x}, -t), \quad (42)$$

$$\mathcal{I}: Q(\mathbf{x}, t) \rightarrow Q(-\mathbf{x}, t) \quad \Delta V(\mathbf{x}, t) \rightarrow -\Delta V(-\mathbf{x}, t). \quad (43)$$

Thus, as stated in the main text, the product is a time-reversal odd pseudoscalar:

$$\mathcal{T}: [Q(\mathbf{x}, t)] [\Delta V(\mathbf{x}, t)] \rightarrow -[Q(\mathbf{x}, -t)] [\Delta V(\mathbf{x}, -t)], \quad (44)$$

$$\mathcal{I}: [Q(\mathbf{x}, t)] [\Delta V(\mathbf{x}, t)] \rightarrow -[Q(-\mathbf{x}, t)] [\Delta V(-\mathbf{x}, t)]. \quad (45)$$

V. DYNAMICAL STRUCTURE FACTOR CALCULATION DETAILS

Here, we sketch the calculation of the dynamical structure factor (DSF) $\mathcal{F}^{ij}(\mathbf{k}, \omega)$, with $i, j = x, y, z$, given by Eq. (7) in the main text. We work at zero temperature with a real time path integral approach and use the notation $\langle \dots \rangle$ to refer to the real time-ordered vacuum expectation value. According to linear response theory, the DSF $\mathcal{F}^{ij}(\mathbf{k}, \omega)$ is given by the imaginary part of the dynamical spin susceptibility. Relating this to the time-ordered correlators, we find

$$\mathcal{F}^{ij}(\mathbf{k}, \omega) = \text{Im} [i \langle S^i(\mathbf{k}, \omega) S^j(-\mathbf{k}, -\omega) \rangle]. \quad (46)$$

Although we use relativistic notation where convenient (with metric $\eta = \text{diag}(1, -1, -1, -1)$ and $c = 1$), the theory is isotropic but not Lorentz invariant. Hence, the tensor symmetry analysis below refers to the rotational 3-tensor structure – not the Minkowski 4-tensor structure, since the theory need not be covariant with respect to boosts.

We recall from main text Eq. (6) that the long-wavelength spin vector field $\mathbf{S} = \mathbf{e} + \frac{\alpha}{\pi} \boldsymbol{\varphi} \mathbf{b}$. Therefore,

$$\begin{aligned} \langle S^i(x) S^j(y) \rangle &= \langle e^i(x) e^j(y) \rangle \\ &+ \frac{\alpha}{\pi} \left[\theta (\langle e^i(x) b^j(y) \rangle + \langle b^i(x) e^j(y) \rangle) + \langle e^i(x) \phi(y) b^j(y) \rangle + \langle \phi(x) b^i(x) e^j(y) \rangle \right] \\ &+ \frac{\alpha^2}{\pi^2} \left[\theta^2 \langle b^i(x) b^j(y) \rangle + \langle b^i(x) \phi(x) b^j(y) \phi(y) \rangle + \theta (\langle b^i(x) \phi(y) b^j(y) \rangle + \langle \phi(x) b^i(x) b^j(y) \rangle) \right], \end{aligned} \quad (47)$$

where we use the notation $x \equiv (t, \mathbf{x})$. As $\langle S^i(\mathbf{k}, \omega) S^j(-\mathbf{k}, -\omega) \rangle$ is a symmetric 2-tensor, the terms linearly proportional to θ must be symmetric 2-pseudotensors. The only symmetric 2-pseudotensors available to construct this correlator are $\theta \delta^{ij}$ and $\theta k^i k^j$. However, as the static θ term is a boundary term, it does not appear in any bulk correlation functions and therefore these terms must vanish. With this simplification,

$$\begin{aligned} \langle S^i(x) S^j(y) \rangle = & \langle e^i(x) e^j(y) \rangle + \frac{\alpha}{\pi} [\langle e^i(x) \phi(y) b^j(y) \rangle + \langle \phi(x) b^i(x) e^j(y) \rangle] \\ & + \frac{\alpha^2}{\pi^2} [\theta^2 \langle b^i(x) b^j(y) \rangle + \langle b^i(x) \phi(x) b^j(y) \phi(y) \rangle]. \end{aligned} \quad (48)$$

The correlators follow from the low-energy effective action using the path integral

$$\mathcal{Z} = \int \mathcal{D}a \mathcal{D}\phi \exp [iS_{\text{eff}}]. \quad (49)$$

Rewriting the effective action in the main text, Eq. (1), in terms of the gauge field a , we have

$$S_{\text{eff}} = \frac{1}{2} \int d^4x \left\{ a^\mu (\eta_{\mu\nu} \partial_\rho \partial^\rho) a^\nu - J\phi (\partial_t^2 - v^2 \nabla^2 + \Delta^2) \phi + \frac{\alpha}{\pi} (\theta + \phi) \epsilon^{\mu\nu\rho\sigma} \partial_\mu a_\nu \partial_\rho a_\sigma \right\}. \quad (50)$$

The first term is the Maxwell Lagrangian, where we used the Faddeev-Popov gauge fixing procedure, choosing to work in the Feynman gauge. The third term is the axion term, where $\epsilon^{\mu\nu\rho\sigma}$ is the totally anti-symmetric Levi-Civita symbol satisfying $\epsilon_{0123} = -\epsilon^{0123} = 1$. From S_{eff} , the free photon propagator in momentum space is given by

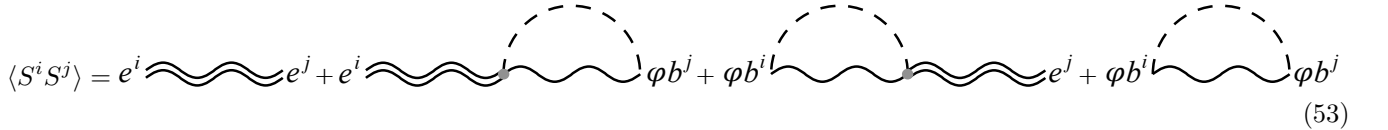
$$D_0^{\mu\nu}(k) = \frac{-i\eta^{\mu\nu}}{\omega^2 - |\mathbf{k}|^2 + i0^+} \quad (51)$$

while the free axion propagator is

$$\Delta_F(k) = \frac{iJ^{-1}}{\omega^2 - v^2|\mathbf{k}|^2 - \Delta^2 + i0^+}, \quad (52)$$

where we use the notation $k \equiv (\omega, \mathbf{k})$.

We proceed by perturbatively evaluating the correlation functions in Eq. (48) to find $\langle S^i(x) S^j(y) \rangle$ to leading loop order. Schematically, we evaluate in the following approximation



$$\langle S^i S^j \rangle = e^i \text{---} e^j + e^i \text{---} \phi b^j + \phi b^i \text{---} e^j + \phi b^i \text{---} \phi b^j \quad (53)$$

where the renormalized photon propagator $D^{\mu\nu}$ is given by solving the Schwinger-Dyson equation,



$$\text{---} = \text{---} + \text{---} \text{---} \text{---} \quad (54)$$

The vacuum polarization tensor (the photon self-energy), $\Pi_{\rho\sigma}(k)$ is given by

$$i\Pi^{\mu\nu}(k) = -\frac{\alpha^2}{\pi^2} \int \frac{d^4p}{(2\pi)^4} \epsilon^\mu{}_{\alpha\tau} \epsilon^\nu{}_{\beta\gamma\lambda} k^\alpha k^\beta p^\tau p^\gamma \Delta_F(k-p) D_0^{\lambda\delta}(p). \quad (55)$$

Because $\Pi_{\rho\sigma}(k)$ is transverse — $k_\mu \Pi^{\mu\nu} = 0$ — and our theory is rotationally invariant, we can write the polarization tensor as

$$\Pi^{\mu\nu} = \Pi_1(\omega, |\mathbf{k}|) P_1^{\mu\nu} + \Pi_2(\omega, |\mathbf{k}|) P_2^{\mu\nu}, \quad (56)$$

where we define the orthogonal projectors — $(P_\ell)^\mu{}_\sigma (P_{\ell'})^{\sigma\nu} = \delta_{\ell\ell'} (P_\ell)^{\mu\nu}$, where $\ell, \ell' = 1, 2$ —

$$P_1^{\mu\nu} = \begin{pmatrix} 0 & \mathbf{0} \\ \mathbf{0} & \frac{k^i k^j}{|\mathbf{k}|^2} - \delta^{ij} \end{pmatrix} \quad (57)$$

$$P_2^{\mu\nu} = \frac{1}{|\mathbf{k}|^2 - \omega^2} \begin{pmatrix} |\mathbf{k}|^2 & \omega \mathbf{k} \\ \omega \mathbf{k} & \omega^2 \frac{k^i k^j}{|\mathbf{k}|^2} \end{pmatrix}, \quad (58)$$

and Π_1 and Π_2 are rotational scalars. Expanding the dressed photon-propagator $D^{\mu\nu}$ in terms of these projectors and $P_3^{\mu\nu} = \eta^{\mu\nu} - P_1^{\mu\nu} - P_2^{\mu\nu}$, Eq. (54) yields

$$D^{\mu\nu} = \frac{-iP_1^{\mu\nu}}{\omega^2 - |\mathbf{k}|^2 - \Pi_1 + i0^+} + \frac{-iP_2^{\mu\nu}}{\omega^2 - |\mathbf{k}|^2 - \Pi_2 + i0^+} + \frac{-iP_3^{\mu\nu}}{\omega^2 - |\mathbf{k}|^2 + i0^+}. \quad (59)$$

The weights Π_1 and Π_2 can be found by considering the trace of Π , yielding

$$\Pi^\mu{}_\mu = 2\Pi_1 + \Pi_2, \quad (60)$$

and the 00 component

$$\Pi^{00} = \frac{|\mathbf{k}|^2}{|\mathbf{k}|^2 - \omega^2} \Pi_2. \quad (61)$$

Solving for Π^{00} and $\Pi^\mu{}_\mu$ using Eq. (55), we find the integral forms

$$i\Pi_1 = \frac{\alpha^2}{J\pi^2} \int \frac{d^4 p}{(2\pi)^4} \left((\omega^2 - |\mathbf{k}|^2)(p_0^2 - |\mathbf{p}|^2) - (p_0\omega - \mathbf{k} \cdot \mathbf{p}) \right. \\ \left. + \frac{1}{2}(\omega^2 - |\mathbf{k}|^2)|\mathbf{p}|^2(1 - \cos^2(\theta)) \right) \Delta_F(k-p) D_0(p), \quad (62)$$

$$i\Pi_2 = \frac{\alpha^2}{J\pi^2} \int \frac{d^4 p}{(2\pi)^4} (\omega^2 - |\mathbf{k}|^2)|\mathbf{p}|^2(\cos^2(\theta) - 1) \Delta_F(k-p) D_0(p), \quad (63)$$

where θ is the polar angle between \mathbf{k} and \mathbf{p} and $D_0(p)$ is defined by $D_0^{\mu\nu}(p) \equiv \eta^{\mu\nu} D_0(p)$.

Given the photon propagator and the axion propagator, we can return to Eq. (48) and calculate each term in momentum space using the definitions $e^i = \partial^i a^0 - \partial^0 a^i$ and $b^i = \epsilon^{ijk} \partial_j a^k$. Under the approximation where only external photon propagators are dressed, Eq. (53), we find

$$\langle e^i(k) e^j(-k) \rangle = k^i k^j D^{00} - \omega k^j D^{i0} - \omega k^i D^{j0} + \omega^2 D^{ij}, \quad (64)$$

$$\langle b^i(k) b^j(-k) \rangle = \epsilon^{imn} \epsilon^{jlp} k^m k^l D^{np}, \quad (65)$$

$$\langle [b^i \phi](k) [b^j \phi](-k) \rangle = \int \frac{d^4 p}{(2\pi)^4} (p^i p^j - \delta |\mathbf{p}|^2) D_0(p) \Delta_F(k-p), \quad (66)$$

$$\langle e^i(k) [\phi b^j](-k) \rangle + \langle [\phi b^i](k) e^j(-k) \rangle = i \frac{\alpha}{\pi} \epsilon^{\tau\lambda\rho n} [\epsilon^{0jln} (k^i D_\lambda^0 - \omega D_\lambda^i) + i \leftrightarrow j] k_\tau \\ \times \int \frac{d^4 p}{(2\pi)^4} p_\rho p^\ell \Delta_F(k-p) D_0(p). \quad (67)$$

Plugging in the expression for the dressed photon propagator, Eq. (59), and simplifying yields

$$\langle e^i(k) e^j(-k) \rangle = \left(\frac{i\omega^2}{\omega^2 - |\mathbf{k}|^2 - \Pi_1 + i0^+} \right) P_T^{ij} + \left(\frac{i(\omega^2 - |\mathbf{k}|^2)}{\omega^2 - |\mathbf{k}|^2 - \Pi_2 + i0^+} \right) P_L^{ij}, \quad (68)$$

$$\langle b^i(k) b^j(-k) \rangle = \left(\frac{i|\mathbf{k}|^2}{\omega^2 - |\mathbf{k}|^2 - \Pi_1 + i0^+} \right) P_T^{ij}, \quad (69)$$

$$\langle [b^i \phi](k) [b^j \phi](-k) \rangle = \int \frac{d^4 p}{(2\pi)^4} (p^i p^j - \delta |\mathbf{p}|^2) D_0(p) \Delta_F(k-p), \quad (70)$$

$$\langle e^i(k) [\phi b^j](-k) \rangle + \langle [\phi b^i](k) e^j(-k) \rangle = \frac{\alpha}{\pi} \int \frac{d^4 p}{(2\pi)^4} \left[\frac{\left(1 - \frac{\omega^2}{|\mathbf{k}|^2}\right) \left((k^i p^j + p^i k^j) \mathbf{p} \cdot \mathbf{k} - 2k^i k^j |\mathbf{p}|^2 \right)}{\omega^2 - |\mathbf{k}|^2 - \Pi_2 + i0^+} \right. \\ \left. + \frac{2\omega \left(\delta^{ij} (|\mathbf{p}|^2 \omega - \mathbf{k} \cdot \mathbf{p} p_0) - \frac{|\mathbf{p}|^2 \omega}{|\mathbf{k}|^2} k^i k^j - \omega p^i p^j + (p_0 - \frac{\mathbf{k} \cdot \mathbf{p} \omega}{|\mathbf{k}|^2}) \left(\frac{k^i p^j + p^i k^j}{2} \right) \right)}{\omega^2 - |\mathbf{k}|^2 - \Pi_1 + i0^+} \right] D_0(p) \Delta_F(k-p). \quad (71)$$

In Eqs. (68) and (69), we have introduced the longitudinal and transverse projectors

$$P_L^{ij} = \frac{k^i k^j}{|\mathbf{k}|^2} \quad (72)$$

$$P_T^{ij} = \delta^{ij} - \frac{k^i k^j}{|\mathbf{k}|^2}, \quad (73)$$

respectively.

Because all these expressions are symmetric 2-tensors, on symmetry grounds they must have the general form

$$M^{ij} = M^L P_L^{ij} + M^T P_T^{ij}, \quad (74)$$

where M^L and M^T are rotational scalars. Eqs. (68) and (69) are already in this form. For Eqs. (70) and (71), by considering the trace and the 33 component of each expression, we can find integral expressions for the respective M^L and M^T weights. In what follows, we assume that the real part of the polarization tensor Π , which renormalizes the dispersion, is zero — i.e., that the dispersion parameters are already renormalized. We consistently drop all other UV-divergent contributions.

To compute the DSF, we take the real part of Eqs. (68-71) in the expression for Eq. (74). Computing the relevant loop integrals using the Cutkosky rules, we find that the structure factor has two different functional forms depending on the energy regime. For energies below the threshold energy

$$\omega_{\text{th}} = \begin{cases} \omega_\phi(\mathbf{k}) & |\mathbf{k}| < k_c \\ \omega_\gamma(|\mathbf{k}| - k_c) + \omega_\phi(k_c) & |\mathbf{k}| \geq k_c \end{cases}, \quad (75)$$

where $k_c = \Delta/(v\sqrt{v^2 - 1})$, the DSF is given by

$$\mathcal{F}^{ij} \Big|_{\omega < \omega_{\text{th}}} = P_T^{ij} \left(\pi + \frac{\alpha^2 \theta^2}{\pi} \right) \omega^2 \delta(\omega^2 - |\mathbf{k}|^2). \quad (76)$$

Above the threshold energy, the DSF instead takes the form

$$\begin{aligned} \left(\frac{\alpha^2}{J\pi^2} \right)^{-1} \mathcal{F}^{ij} \Big|_{\omega > \omega_{\text{th}}} &= P_L^{ij} \left(1 - \frac{(\omega^2 - |\mathbf{k}|^2)^2}{(\omega^2 - |\mathbf{k}|^2)^2 + \alpha^4 J^{-2} I_2^2} \right) M_{b\phi b\phi}^L \\ &+ P_T^{ij} \left[\frac{I_1 \pi^2 \left(\omega^2 + \frac{\alpha^2 \theta^2}{\pi^2} |\mathbf{k}|^2 \right) + (\omega^2 - |\mathbf{k}|^2) M_{eb\phi}^T}{(\omega^2 - |\mathbf{k}|^2)^2 + \alpha^4 J^{-2} I_1^2} + M_{b\phi b\phi}^T \right]. \end{aligned} \quad (77)$$

In this expression, the quantities I_1 , I_2 , $M_{b\phi b\phi}^L$, $M_{b\phi b\phi}^T$, and $M_{eb\phi}^T$ are given by the integrals

$$I_1 = -\frac{1}{16\pi^3 v^2 |\mathbf{k}|} \int_{p_-}^{p_+} dp p^2 \left(\frac{\omega^2 - |\mathbf{k}|^2}{2} (1 - f(p)^2) - (\omega - kf(p))^2 \right), \quad (78)$$

$$I_2 = -\frac{1}{16\pi^3 v^2 |\mathbf{k}|} \int_{p_-}^{p_+} dp p^2 (\omega^2 - |\mathbf{k}|^2) (f(p)^2 - 1), \quad (79)$$

$$M_{b\phi b\phi}^L = -\frac{1}{16\pi v^2 |\mathbf{k}|} \int_{p_-}^{p_+} dp p^2 (f(p)^2 - 1), \quad (80)$$

$$M_{b\phi b\phi}^T = -\frac{1}{16\pi v^2 |\mathbf{k}|} \int_{p_-}^{p_+} dp p^2 \left(\frac{-1 - f(p)^2}{2} \right), \quad (81)$$

$$M_{eb\phi}^T = -\frac{1}{16\pi v^2 |\mathbf{k}|} \int_{p_-}^{p_+} dp p^2 (\omega^2 - 2|\mathbf{k}|\omega f(p) + \omega^2 f(p)^2), \quad (82)$$

where the function $f(p)$ is given by

$$f(p) = \frac{v^2 |\mathbf{k}|^2 + \Delta^2 + (p + pv - \omega)(-p + pv + \omega)}{2|\mathbf{k}|pv^2} \quad (83)$$

and the bounds on the integrals are

$$p_- = \begin{cases} \frac{v^2|\mathbf{k}| - \omega - \sqrt{\Delta^2 + v^2(|\mathbf{k}| - \Delta - \omega)(|\mathbf{k}| + \Delta - \omega)}}{v^2 - 1} & v > 1 \text{ and } \omega < \omega_\varphi(\mathbf{k}) \\ \frac{-v^2|\mathbf{k}| - \omega + \sqrt{\Delta^2 + v^2(|\mathbf{k}| - \Delta + \omega)(|\mathbf{k}| + \Delta + \omega)}}{v^2 - 1} & \omega > \omega_\varphi(\mathbf{k}) \end{cases}, \quad (84)$$

$$p_+ = \frac{v^2|\mathbf{k}| - \omega + \sqrt{\Delta^2 + v^2(|\mathbf{k}| - \Delta - \omega)(|\mathbf{k}| + \Delta - \omega)}}{v^2 - 1}. \quad (85)$$

Because the spin field is divergence free, the correlation function and thus the DSF should be purely transverse. We see that to leading order in α^2/J , the longitudinal component of Eq. (77) indeed vanishes, leaving only the transverse part. However, at high-orders of α^2/J this is not the case, which is an unphysical byproduct of our finite order perturbative treatment. Therefore, we finally drop the longitudinal part to arrive at the expression for the DSF studied in the main text:

$$\mathcal{F}^{ij} \Big|_{\omega > \omega_{\text{th}}} = \left(\frac{\alpha^2}{J\pi^2} \right) P_T^{ij} \left[\frac{I_1 \pi^2 \left(\omega^2 + \frac{\alpha^2 \theta^2}{\pi^2} |\mathbf{k}|^2 \right) + (\omega^2 - |\mathbf{k}|^2) M_{e\bar{b}\bar{b}\phi}^T}{(\omega^2 - |\mathbf{k}|^2)^2 + \alpha^4 J^{-2} I_1^2} + M_{b\phi b\bar{b}}^T \right]. \quad (86)$$